Journal of Manufacturing Processes 71 (2021) 753–762

Contents lists available at ScienceDirect

Journal of Manufacturing Processes

journal homepage: www.elsevier.com/locate/manpro

Frontal polymerization-assisted 3D printing of short carbon fibers/dicyclopentadiene composites

Zimeng Zhang [a,1], Ruochen Liu [b,1], Wei Li [a], Yuchen Liu [a], Zhijian Pei [a], Jingjing Qiu [c], Shiren Wang [a,b,*]

[a] Department of Industrial and Systems Engineering, Texas A&M University, College Station, TX 77843, USA
[b] Department of Materials Science and Engineering, Texas A&M University, College Station, TX 77843, USA
[c] Department of Mechanical Engineering, Texas Tech University, Lubbock, TX 77409, USA

ARTICLE INFO

Keywords:
Frontal polymerization
3D printing
Thermosetting composites
Interlayer bonding

ABSTRACT

Discontinuous carbon fibers (d-CFs) with different surface modifications (sizing, carboxyl-grafting, and norbornene-grafting) were separately dispersed in dicyclopentadiene (DCPD) resins, and the resultant d-CF/DCPD mixtures demonstrated shear-thinning characteristics. Subsequently, d-CF/DCPD mixtures were printed and further transformed into crosslinked polymers through self-propagating frontal polymerization. The norbornene groups grafted on the d-CF surfaces also reacted with the DCPD monomers during the fontal polymerization-synchronized printing, resulting in covalent connections between d-CFs and DCPD resins. The tensile strength of as-printed norbornene-grafting d-CFs/DCPD composites was around 43.3 MPa, which was 170% higher than that of as-printed neat DCPD resin and 15% higher than that of the sized d-CFs/DCPD composites. The toughness of as-printed norbornene-grafting d-CFs/DCPD composites was ~14 MPa, ~33.3% higher than that of the sized d-CF/DCPD composites. More importantly, the presence of norbornene-grafted d-CFs significantly strengthened the bonding strength of printed layers since d-CFs bridged two neighbored layers. The bonding strength of printed layers was enhanced by ~255% with addition of 3 wt% norbornene-grafting d-CFs compared to the neat resin. This method provides a new way to improve the interlayer bonding in energy-efficient 3D printing thermosetting composites.

1. Introduction

Thermosetting polymers demonstrate outstanding mechanical properties, thermal-resistance and chemical-resistance, and have been extensively used in many industries, including aerospace, automotive, marine industries [1–3]. Conventionally, thermosetting polymers are fabricated by molding with a secondary curing process. However, the use of mold makes it difficult to construct complex geometry [4] and also increases the manufacturing cost, especially for customized requests. The emerging additive manufacturing techniques offer design flexibility, ease-of-process, and print-on-demand, and have a great potential to transform thermoset manufacturing [5–11]. Stereolithography (SLA) and digital light processing (DLP) are limited to photo-curable materials. In addition, the limited light penetration depth may cause incomplete cure and thus post curing is needed [12,13]. Other thermally cured resins usually undergo two-step fabrication process: printing the structure and subsequently ex-situ thermal curing in ovens or autoclaves. Such ex-situ curing at high temperature and extended curing time (usually several hours) after structure formation consumes an excessive amount of energy [14,15]. For example, curing Boeing 787 fuselage takes 8 h, consumes 350 gigajoules (GJ) energy, and produces 80 tons of carbon dioxide [16]. Therefore, one-step energy-efficient manufacturing of high-performance thermosetting polymers is highly desired for environmental and economical purposes.

Frontal polymerization-assisted printing provides a rapid and energy-efficient way for thermosetting polymer fabrication. During the frontal polymerization, the polymerization was initiated with a small amount of transient external heat and then propagated in a reaction wave, transforming monomers to crosslinked polymers without further external energy supply [17,18]. The heat released from the previous reaction zone dissipates to the nearby region [19–21], and thus the reaction continuously propagates automatically [22]. With the depletion

* Corresponding author at: Department of Industrial and Systems Engineering, Texas A&M University, College Station, TX 77843, USA.
E-mail address: s.wang@tamu.edu (S. Wang).
[1] These authors have equal contributions.

https://doi.org/10.1016/j.jmapro.2021.10.014
Received 19 March 2021; Received in revised form 6 October 2021; Accepted 8 October 2021
Available online 19 October 2021

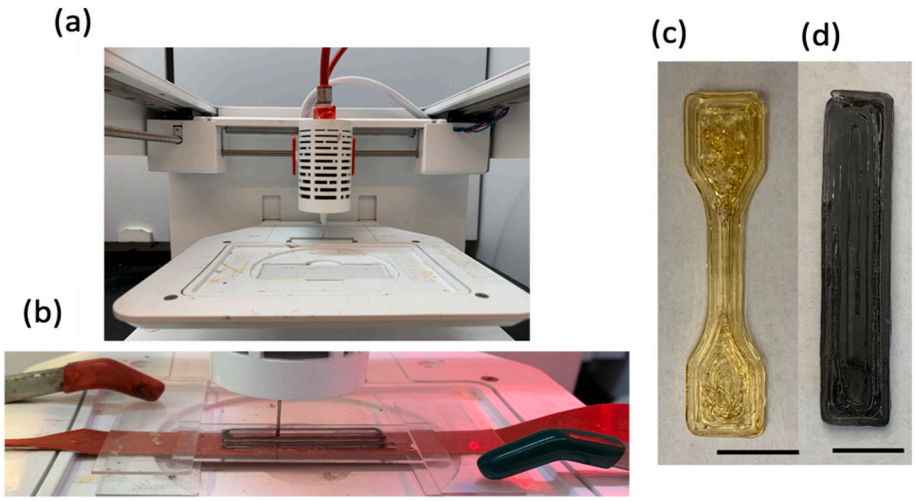

Fig. 1. Extrusion-based printer setup and printing demonstration; (a) printer set up (commercially available printer Allevi 1); (b) CF composites printing demonstration. A flexible heater (red belt beneath the glass substrate) was used to initialize the frontal polymerization; (c) printed virgin poly(DCPD) tensile bar; (d) as-printed CF composites cuboid. Scale bar: 10 mm. (For interpretation of the references to color in this figure legend, the reader is referred to the web version of this article.)

of reactive monomers or initiators, the propagation stopped. Frontal polymerization has been studied over for 40 years, providing a simpler and more affordable way of fabrication [23,24]. A wide range of monomers have been applied to frontal polymerization including vinyl monomers [25], methacrylate [26], polyurethane [27], bisphenol A epoxy [28], dicyclopentadiene [23,29,24] and epoxy-urethane [30], and so on. The initiation process can be implemented by external heat or light. One typical example is frontal ring-opening metathesis polymerization of dicyclopentadiene (DCPD) with the presence of highly efficient ruthenium Grubbs'-type II (GC2) catalyst [31]. White et al. integrated frontal ring-opening metathesis polymerization of DCPD into extrusion printing, resulting in the one step rapid manufacturing of DCPD-based polymers [32]. Simulation study regarding DCPD frontal polymerization were also reported [20,21]. Our previous study also proved the feasibility of print and in-situ polymerization with optimal process parameters and material formulation [33]. As a result, DCPD with efficient catalysts is a high desirable material for rapid prototyping.

Thermosetting composites with micro- or nano-scale fillers are extensively used as structural materials in harsh environment and extreme conditions [34]. Previous studies reported improvements in mechanical properties [35], fire retardancy [36], and prevention of oxidation [37] through inclusion of discontinuous carbon fibers(CFs) into thermosetting polymers. However, filler/DCPD composites remain underexplored. Computation modeling of unidirectional filler-incorporated composites in a DCPD matrix was reported. [38,39] Vyas et al. compared the mechanical properties of the composites produced by frontal polymerization with those of composites produced by bulk polymerization using the heat transfer model along with *n-th* order reaction kinetics model. [39] Besides the computational modeling, frontal polymerization-assisted bulk fiber-incorporated DCPD thermoset composites fabrication was reported [32]. To the best of our knowledge, no attempt has been made to examine the interlayer bonding strength for frontal polymerization-assisted thermoset printing.

In this paper, discontinuous CFs with different surface modifications were integrated into DCPD resins with the presence of second-generation Grubbs' catalyst (GC2) and underwent direct writing via frontal polymerization. The filler incorporated DCPD resins generated shear thinning behavior that facilitated the printing process. The mechanical properties of as-printed CFs-incorporated composites were analyzed and compared. Besides, the interlayer bonding strength of neat DCPD, CFs/DCPD composites and functionalized-CF/DCPD composites were explored. The effects of CF surface chemistry on the interlayer bonding of printed DCPD-based composites were discussed.

2. Experimental

2.1. Materials

Dicyclopentadiene (DCPD), 5-ethylidene-2-norbornene (ENB), phenylcyclohexane (PC), acetone, and triethyl phosphite (TEP) inhibitor were purchased from Sigma-Aldrich. The second-generation Grubbs' catalyst (GC2) was purchased from Chem-Impex International (“CII”). 5-norbornene-2-carboxylic acid was purchased from Sigma-Aldrich. Other chemicals used in norbornene/ carbon fiber functionalization including thionyl chloride ($SOCl_2$), triethylamine (Et_3N), pentaerythritol, dimethylformamide (DMF), Dichloromethane (DCM), acetone, were purchased from Acorn, VWR, and Sigma-Aldrich, respectively. All the chemicals were used as received. Discontinuous carbon fiber (d-CFs, T800) with an 8-um diameter was kindly provided by National Aeronautics and Space Administration (NASA).

2.2. CFs surface modifications

2.2.1. Desizing CFs and surface oxidation

100 mg carbon fiber was soaked in 250 ml acetone and refluxed at 80 °C for 24 h. Fibers were coated with sizing materials to protect the fibers prior to further applications. Desizing process aimed to remove the sizing materials from the fibers to expose the fiber surface for chemical modifications. The desized fibers were washed with DI water to remove residuals and to adjust the pH value to neutral. Desized CFs were then treated with HNO_3 (67%, 100 mL) bath sonication for 15 min, and d-CFs were subsequently refluxed at 100 °C for 6 h to prepare carboxyl functionalization. As-treated CFs were washed with deionized (DI) water to remove the residual acid and neutralize pH value, and then dried in vacuum oven to obtain carboxyl-functionalized CF.

2.2.2. Synthesis of triol-functionalized CF

the carboxyl-functionalized CFs (44 mg) were refluxed in an excess amount of $SOCl_2$ and a catalytic amount of DMF under N_2 at 70 °C for 36 h to form acyl chloride. The synthesis was operated using a Schlenk line under N_2 protection. Later thionyl chloride was removed. Pentaerythritol (1.14 g) and 10 ml THF were treated with the acyl chloride for 36 h at 70 °C and washed with 300 mL dichloromethane (DCM) and 100 mL THF alternatively to remove the chemicals that left on the d-CFs during the synthesis. As-functionalized fibers were then dried under vacuum and then collected for characterization and printing.

2.2.3. Synthesis of norbornene-functionalized CFs

The 5-norbornene-2-carboxylic acid (6.0 mL) was mixed with an

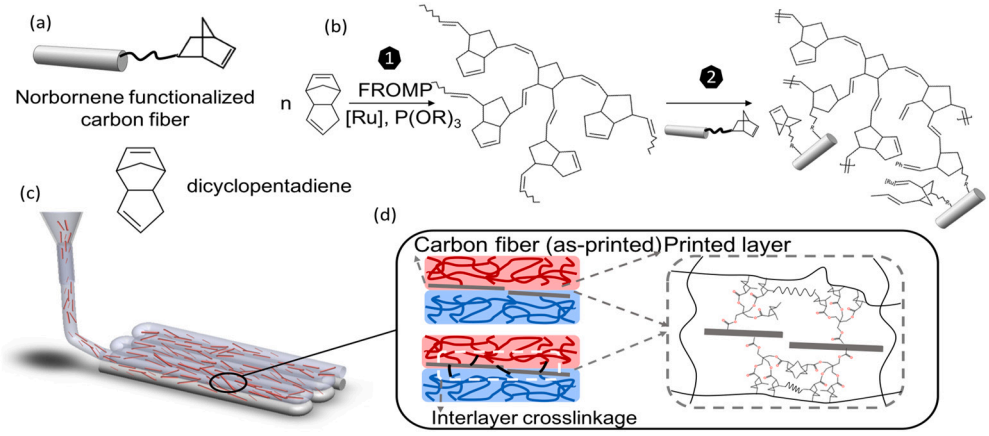

Fig. 2. Illustration of frontal polymerization-enabled printing and interlayer bonding; (a) chemical structure of grafted norbornene group and monomer dicyclopentadiene used as polymer matrix; (b) Scheme of functionalized CF based self-reinforcement. Step 1: FROMP of poly(DCPD); Step 2: chemical crosslinking of functionalized CFs to poly(DCPD) matrix; (c), (d) Schematic illustration of functionalized CF reinforcement through in-situ interlayer bonding.

excess amount of thionyl chloride in a flask and stirred under N_2 protection for 24 h to form acyl chloride. Then excess thionyl chloride was evaporated and cooled to room temperature. After the removal of thionyl chloride, the triol-functionalized CFs were added with the addition of DCM, anhydrous DMF, and triethylamine. The acyl substitution was proceeded under N_2 protection for another 48 h at 50 °C and washed with 300 mL dichloromethane (DCM) and 100 mL THF alternatively to remove the residual chemicals. Then, norbornene-functionalized CFs were oven-dried. Schlenk set up used in the synthesis is shown in Fig. S1.

Sized, desized, hydroxy-functionalized and norbornene-functionalized CFs were characterized by FTIR (potassium bromide [KBr] pellet). The morphology of the CFs after synthesis were characterized by optical microscopy.

2.3. Inks preparation

To realize printing and in-situ curing of DCPD/CF composites, DCPD resin was first prepared by following Robertson et al.'s procedure with modifications [16]. Specifically, to reduce the melting point of DCPD solution to below the room temperature, 5 wt% 5-ethylidene-2-norbornene (ENB) was added to Dicyclopentadiene (DCPD) at 40 °C. Second-generation Grubbs' catalyst (GC2) was dissolved in phenylcyclohexane (PC) to obtain 1 wt% GC2 solution. The inhibitor, triethyl phosphite (TEP), was added to PC to obtain 10 vol% TEP solution. The ink was prepared by mixing 6.4 µl TEP and 341 µl GC2 with 5 g DCPD. As a result, the molar ratio of DCPD, GC2 and TEP in the ink is 10,000:1:1. The mixture was degassed and stored at room temperature for 2 h before the printing. For the preparation of CFs-incorporated DCPD ink, CFs were first dispersed in DCPD at 40 °C via bath sonication for 10 min and then stirred for 2 h.

2.4. 3D printing

The digital model of composite parts was firstly created using CAD tools and then converted into motion commands in 3D spaces for the printer. A 3D printer (Allevi 1, Fig. 1a) was used to print DCPD/CF composites. A flexible heater (New Era, 33 W, 2 thermocouple, 90 cm cord, 1.5 cm x50cm flat to spiral heating pad) was placed beneath the substrate as a heat supply for reaction activation. The 18-gauge needles were used at a printing speed of 2 mm/s. The printer has a printing accuracy of 7.5 um in X-, Y-axis, and 1 um in *Z*-axis. The printer has a build volume of 90 × 60 × 130 mm. The printer can be auto-calibrated every time before the print job starts. A pneumatic pump was used for material extrusion. The extruder head can hold a 5 ml cartridge. The extrusion pressure can be adjusted by tuning the pneumatic flow. Commercial nozzles can be inserted on the other end of the cartridge to acquire specific print accuracy. Flexible heater was also incorporated in the extruder head for ink temperature control before printing. It can control the temperature in the range of 4 °C to 160 °C. The inks were loaded in the syringe, kept at 4 °C for printing. The frontal polymerizable ink is forced out of the nozzle tip and deposited onto the substrate. Heater underneath the glass substrate was set to 85 °C as the heat supply for initiation. The printing speed was adjusted to match the frontal reaction. The polymerization front was noticeable where polymer turned yellow after polymerization. For CF/DCPD composites, it was hard to distinguish from color, but the polymer turned glossy on the surface after crosslinking. Fig. 1b shows a demonstration of printing and in-situ polymerization of CF/DCPD composites. Fig. 1c and 1d shows the printed neat resin and CF composites. The dimensional accuracy was analyzed by measuring the as-printed part geometry compared to original design. The printed geometry shows a deviation in dimensions within the range of 7%. The dimensions of printed geometry were obtained using caliper, and the measurement and designed geometry are shown in Fig. S2.

2.5. Rheological characterization and DSC characterization

The rheology behavior of the DCPD solution was characterized by Anton Paar Physica MCR-301 rheometer. The DCPD solutions were stored at room temperature/ ice bath for a different period, and then their viscosities and shear stress were measured by a 50 mm CP 50–1 plate geometry. DSC (Q20, TA Instruments) equipped with a CFL-50 cooling system was used for heat of reaction analysis.

2.6. Mechanical tests

ASTM D638 type-V specimens with modified dimensions were prepared for tensile test. Specifically, the dimension of printed tensile specimens is similar to ASTM D638 type-V ones, except the grip area reduced to 10 mm on each side in this study. Instron 3345 tensile machine (Instron Corporation, MA, USA) with 2 kN load cell were used. The cross-section area of the tensile specimens was measured before tensile testing. The tensile test speed was set to 10 mm min^{-1}. Ultimate tensile strength, Young's modulus, and elongation at break were calculated using the strain-stress curve. Interfacial shear test specimen was prepared following ASTM D3163 standard with a modified interfacial area of 10 mm by 6 mm. The overall dimension of the specimen is 90 mm in length and 6 mm in width. The test speed was set to 6 mm min^{-1}. Interfacial shear strength was determined by the maximum loading force per unit interfacial area. All specimens were tested directly after

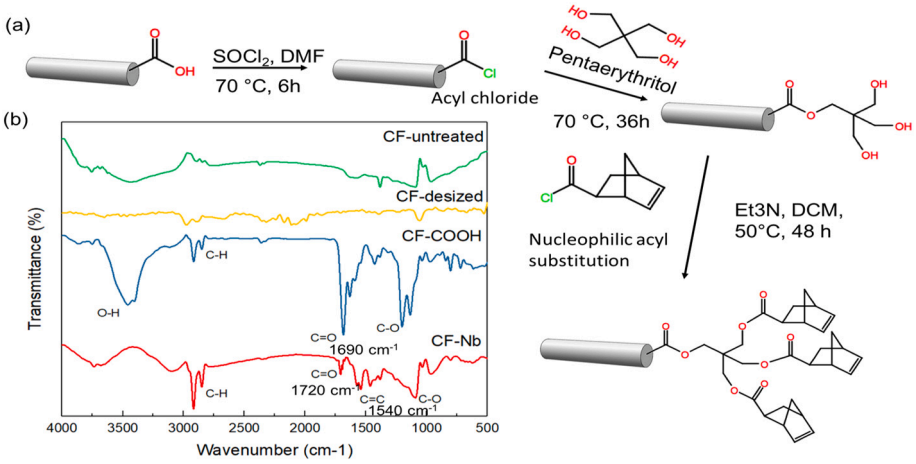

Fig. 3. CF surface modification and FTIR results. (a) Scheme of grafting norbornene onto the CF surface; (b) FTIR results: green, yellow, blue, and red represent untreated (CF-untreated), desized (CF-desized), hydroxy grafted (CF-COOH) and norbornene grafted (CF-Nb) CF. (For interpretation of the references to color in this figure legend, the reader is referred to the web version of this article.)

printing without any post-treatment.

2.7. Morphological characterization

The fracture surface morphology of tensile and interlayer test specimens was characterized by scanning electron microscopy (SEM, JEOL JSM-7500F).

3. Results and discussion

3D printing of CF/DCPD composites with in-situ curing was illustrated in Fig. 1. Specifically, the chemical structure of norbornene functional group and monomer structure of the thermosetting polymer matrix are shown in Fig. 2a. The key concept for improving interlayer adhesion while printing is to introduce the reactive groups onto the fiber surface. During the printing, frontal polymerization occurred spontaneously with the presence of the GCII catalytic system, and polymerization of monomers in the nearby region resulted in highly crosslinked polymer matrix. Some reactive sites from frontal ring-opening metathesis polymerization (FROMP) of highly reactive DCPD remain active for secondary crosslinking of olefin addition, as shown in Step 1 of Fig. 2b. Similarly, when the crosslinked polymer chains approach the reactive norbornene groups on fiber surface that contains the similar chemical structure and shares the same ring-opening reaction route with DCPD monomer, it initiates the FROMP reaction and bridges CF to the propagating DCPD chains as shown in Fig. 2b step 2. As a result, strong covalent bonding between the polymer chain and CFs will be produced. More importantly, since the norbornene group is reacted with the same catalyst of DCPD, the CF reacted with DCPD matrix spontaneously and synchronized with the printing process for adjacent exothermic polymerization, resulting in in-situ bridged CF/matrix interfaces. When the fiber sits between two adjacent filament traces, the generated covalent bonds between fiber and polymer matrix could also be present at the interlayer, as illustrated in Fig. 2c, and thus considerably boost the interfacial bonding as shown in Fig. 2d. The inset drawing (dashed grey box) in Fig. 2d demonstrates the crosslinking networks between fiber and polymer matrix. Obviously, these polymer networks not only create the adhesion between printed layers in the vertical directions but also provide the adhesion between printed layers in the horizontal plane as long as d-CFs crossed two neighbored boundaries. Fiber loading and the large surface to volume ratio of the microscale filler reinforcement provided a large number of reactive sites for crosslinking, resulting in an effective load transfer between CFs and matrix. Moreover, the crosslinking reaction not only happened between polymer matrix and CFs but also occurred among polymer matrices across interlayers, resulting in secondary network of olefin addition, as shown in Fig. 1d. With the assistance of the norbornene functioned fibers, the overall mechanical performance of the 3D printed DCPD CF/DCPD composites could be strengthened while post-treatment was eliminated for rapid, energy-efficient freeform fabrication of high-performance thermosetting composites.

3.1. CF surface modification and characterization

Norbornene-functionalized CFs were synthesized in the following sequence: carboxyl groups, acyl chlorides with subsequent grafting of triol groups, and norbornene group grafting via esterification. The schematic illustration of the modification process is shown in Fig. 3a. Synthesis details were provided in Experimental Section 2.2. Firstly, as-received fibers were immersed in acetone bath and refluxed for 48 h to remove sizing agents and clean the fiber. The clean and desized fibers were further oxidized to graft carboxyl groups. Subsequently, hydroxyl group was grafted using esterification reaction via acyl chloride, a highly reactive intermedia for carboxyl and hydroxyl esterification. Acyl chloride then reacted with pentaerythritol, introducing three primary hydroxyl groups at each carboxyl site on the fiber surface. Similarly, the 5-norbornene-2-carboxylic acid was treated with thionyl chloride to produce norbornene acyl chloride. During the norbornene acyl chloride preparation, the solution color changed to scarlet (shown in Fig. S1a). The norbornene acyl chloride then reacted with the hydroxyl group on fiber surface to form norbornene functionalized CF. After d-CFs were added, the color of the solution turned black due to the presence of CFs, as shown in Fig. S1b. The Schlenk synthesis set up is shown in Fig. S1c. One opening of the three-necked flask was connected with the condenser while the other two were sealed with rubber caps for solution supply. The flask was placed in an oil bath for heating. The other side of the condenser was connected with N_2 gas pipeline and drying tube for anhydrous and anaerobic reaction environment requirements. The norbornene functionalized fibers were dried and could undergo ring-opening polymerization with the presence of GCII, resulting in the formation of covalent bonds between CFs and polymer matrix.

The norbornene functionalization d-CFs were characterized by Fourier-transform infrared spectroscopy (FTIR). The spectra of untreated, desized, carboxyl-functionalized and norbornene-functionalized CFs are shown in Fig. 3b. The broad peak at 3100 to 3700 cm^{-1} corresponded to the -OH stretching of carboxyl groups. The peak at 1690 cm^{-1} was assigned to C═O stretching of carboxyl groups. In contrast, the broad -OH peak disappeared in the norbornene

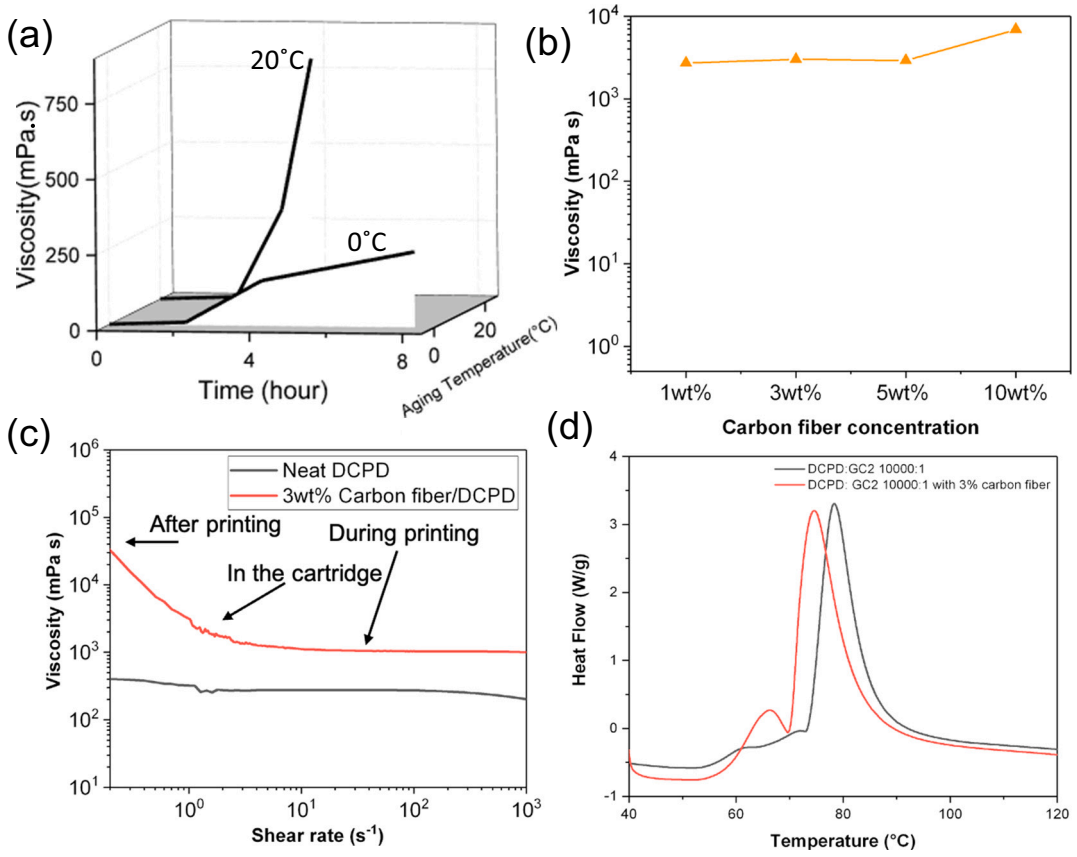

Fig. 4. Rheological behavior and cure kinetics of DCPD and CF-incorporated DCPD ink. (a) Viscosity of neat DCPD ink vs. time (red: stored at room temperature; blue: stored in ice at 0 °C), adapted from our previous publication [33]; (b) viscosity of CF-incorporated DCPD ink vs. CF-loading concentration (measurement shear rate: 1 s-1); (c) viscosity of neat DCPD and 3 wt% CF-incorporated DCPD at different shear rates; (d) DSC analysis of neat DCPD and 3 wt% CF-incorporated DCPD (heated at a constant rate of 10 °C min^{-1}). (For interpretation of the references to color in this figure legend, the reader is referred to the web version of this article.)

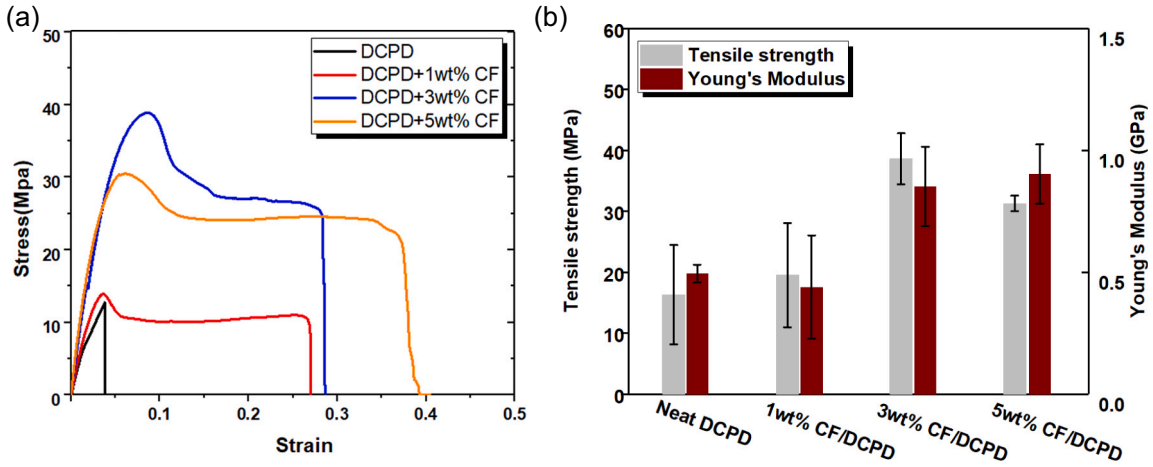

Fig. 5. Effect of CFs on mechanical performance of printed composites; (a) original strain-stress curve of neat DCPD and CF/DCPD composites with different loading; (b) comparison of tensile strength and Young's modulus of DCPD and CF/DCPD composites.

functionalized CFs while a new peak showed at 1540 cm^{-1}, which corresponded to C═C bonds for norbornene groups. Besides, the redshift of C═O bond from 1690 cm^{-1} to 1720 cm^{-1} provided further evidence of the formation of ester.

3.2. Rheological behavior and curing reaction

The rheological behavior of the neat resin and CF-filled resin was measured to determine the ink formulation and process parameters for extrusion printing. The viscosity changed over time since the polymer chains started to form even at 0 °C due to resin's high reactivity with the proposed catalytic system. The viscosity change was due to the chain growth where the increasing chain length increased the ink viscosity. Hence, the ramping rate of viscosity over time was dependent on the polymerization kinetics.

To understand and determine the printing window, rheology and

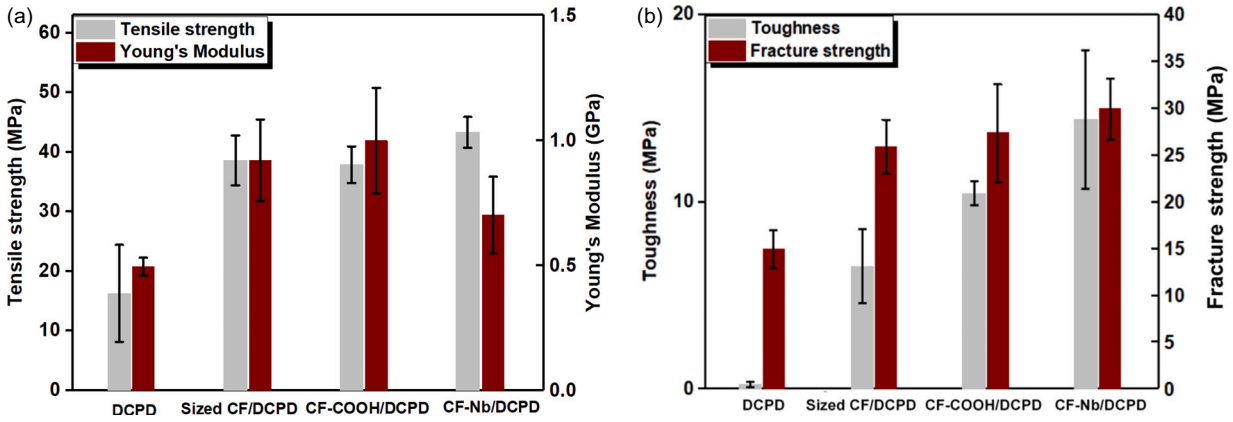

Fig. 6. Effect of CF functionalization on mechanical performance of printed composites; (a) tensile strength and Young's modulus of neat DCPD and DCPD composites with 3 wt% loading; (b) toughness and fracture strength of neat DCPD and DCPD composites. The norbornene grafting was represented with CF-Nb.

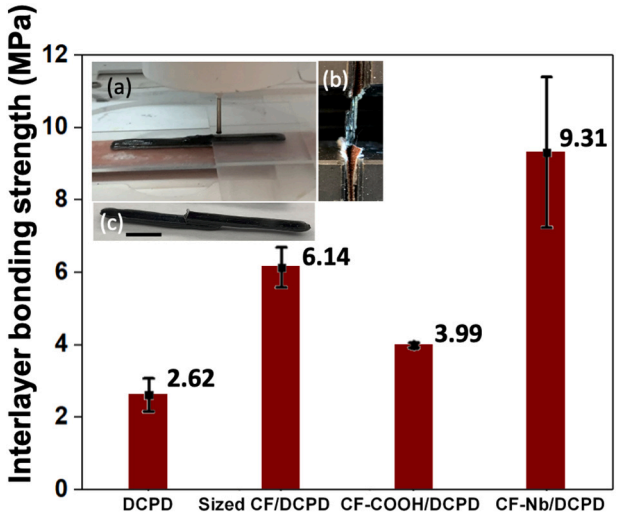

Fig. 7. Effect of fiber surface chemistry on interlayer bonding of printed composites. The norbornene grafting was represented with CF-Nb. Inset image scale bar: 10 mm.

kinetics studies were examined and the results are shown in Fig. 4. The effects of storage time on DCPD viscosity at room temperature (20 °C) and 0 °C are shown in Fig. 4a. Here, the DCPD ink used in this research was formulated with DCPD monomer, GCII catalyst, and inhibitor. The catalyst and inhibitor amount used for printing was based on our previous research [33]. The viscosity of the ink increased dramatically in the first 3–4 h at room temperature, indicating the polymerization started directly after the addition of initiator and inhibitor into the monomer. After the initial 3–4 h of preparation, the ink reached its gel point. A previous study indicated that before reaching the gel point, the ink could exhibit a higher processability for the infusion process where the low-viscosity resin was preferred [32]. This is because the higher viscosity and elasticity induce higher resistance for the extrusion process. The increasing rate of viscosity at 0 °C over time was much slower than that at room temperature, indicating the reaction can be partially inhibited at a lower temperature. Therefore, keeping the ink at a low temperature is an effective way to prevent rapid gelation and extend the printing lifespan. The ink showed a 2 to 3 h process window before turning too viscous to print. According to the viscosity measurement results, DCPD ink was used for printing after the ink was kept at 4 °C for 2 h. Subsequently, the viscosity of CF-loaded resin was also studied at 4 °C. The viscosity of the composite ink was measured after the ink was prepared for 2 h. The shear rate was set to 1 s^{-1} for viscosity measurement.

The addition of CF increased the ink viscosity, as shown in Fig. 4b. A higher CF loading yielded a higher ink viscosity. The fiber ratio studied in this research ranged from 0 to 5 wt%. Because of their high aspect ratio, CFs induced shear thinning behavior, which potentially improved the dimensional accuracy for printing. The shear thinning behavior refers to the decreasing viscosity with increasing shear rate. During extrusion printing, when ink flows into the narrow nozzle tip by pneumatic force, a small-size nozzle induced large pressure against its flow, and thus the decreased viscosity could reduce the resistance and facilitate ink flow. When the ink was squeezed out of the nozzle tip, resistant force disappeared and the shear rate was reduced, the viscosity of the ink could recover at the same time. The demonstration of the rheological behavior of composite ink and the comparison with neat resin are shown in Fig. 4c. The grey and red line represented the viscosities at different shear rates for DCPD and 3 wt% fiber composites, respectively. The viscosity vs. shear rate curve obeyed a power-law model:

$$\eta = K\dot{\gamma}^{n-1}$$

where $\dot{\gamma}$ is the shear rate; K is the consistency index, and n is the power-law index. K represents the value of apparent viscosity of the fluid at a shear rate of 1 s^{-1}, and n indicates the degree of shear thinning behavior [40]. Besides, the shear rate that ink undergoes for different process states, including in the cartridge, during printing, and after printing, can be determined via the following model:

$$\dot{\gamma} = \frac{8\nu}{d}$$

where ν is the printing speed and d is the inside diameter of the cartridge or needle [40]. In this study, the printing speed was 2 and 2.5 mm/ s for neat DCPD and composite ones, respectively. The cartridge's inner diameter was 16 mm, and the needle inner diameter was 838 μm. The corresponding viscosities at different process states were calculated and are shown in Fig. 4b. The CF/DCPD fluids demonstrated obvious shear thinning at $\gamma < 1$ s^{-1}, and then remained at a low viscosity independent of the shear rate.

Fig. 4d shows the Differential Scanning Calorimeter (DSC) analysis of DCPD resin and DCPD composite ink, marked by grey and red line, respectively. From the DSC curve, both neat DCPD ink and DCPD composite ink exhibited high reactivity with an enthalpy of ~224.56 J g^{-1} and ~ 217.44 J g^{-1} calculated by accumulating the area under the curve, respectively. With the addition of d-CFs, the exothermic peak slightly shifted to a lower temperature, indicating the formulation becomes more reactive with the addition of CFs. More specifically, the curing reaction achieved a peak rate at a lower temperature. Based on Arrhenius equation [12,17,21,22], k = Aexp(−E/RT), A: material

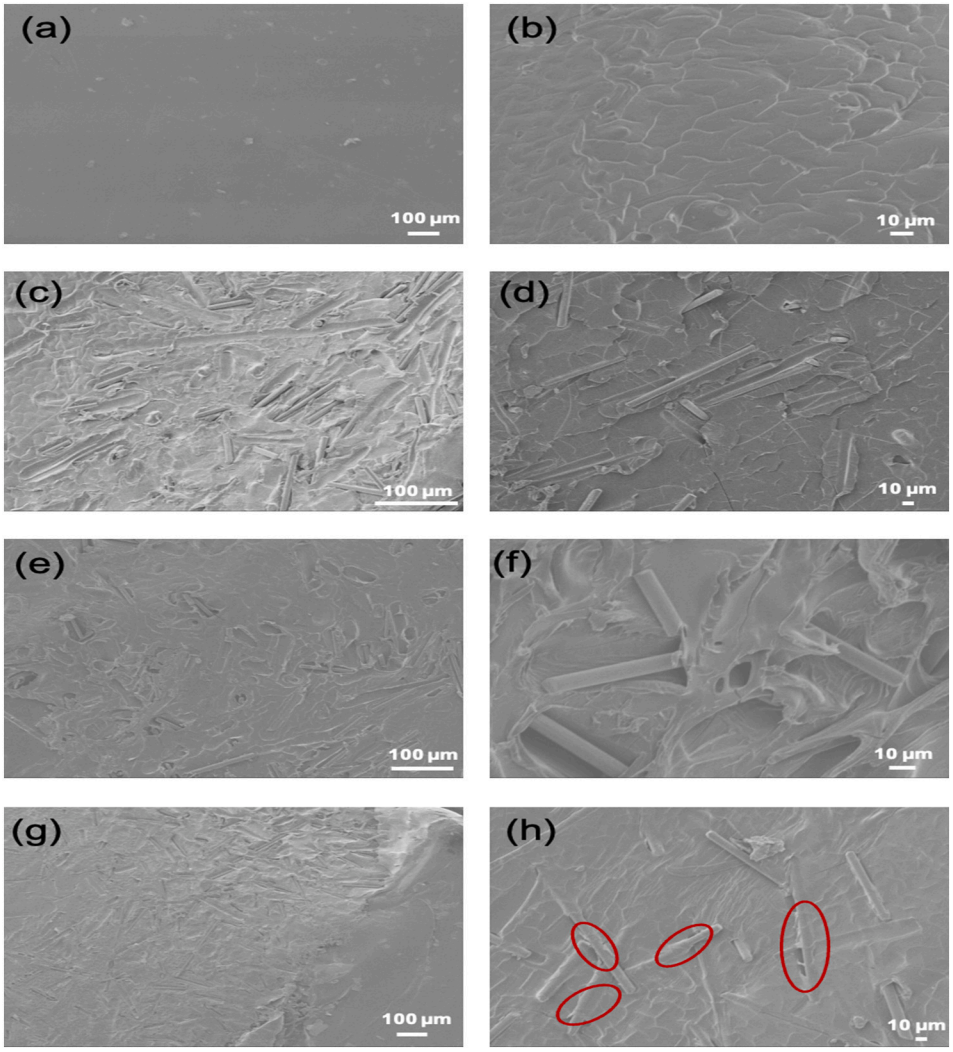

Fig. 8. SEM images of interfacial shear test fracture surface of (a,b) neat DCPD; (c,d) sized CF/DCPD; (e,f) CF-COOH/DCPD; (g,h) CF-Nb/DCPD.

constant, k: reaction rate constant, E: activation energy, T: reaction temperature, and R: ideal gas constant, the curing should show a low activation energy, and thus it is more reactive. We assume that the norbornene group on d-CFs' surface helps decrease the activation energy of the reaction, that helps to reduce the reaction temperature. The peak of CF loaded resin was slightly lower than that of neat DCPD because the highly thermal conductive fiber facilitates thermal transport and speeds up the frontal polymerization process.

3.3. Tensile test

The effect of CF fractions on tensile strength and tensile modulus of the printed composites was analyzed. Tensile specimens were printed while the ink formulation was described in Section 2.2 and printing procedure was introduced in Section 2.3 and 2.4. For tensile specimen printing, filaments were extruded and cured after deposited onto the platform and bonded to the previous printed adjacent filaments. The inset picture of Fig. 5b shows printed CF/DCPD tensile bars (left) and broken bars after tensile testing (right). Neat DCPD and CF/DCPD composites with different fiber fractions were printed and tested. The CF fractions were set to 1 wt%, 3 wt% and 5 wt%. Tensile bars were gripped by the load cells with sandpaper placed between to increase friction for the grips. Typical strain-stress curves of printed thermosets and composites specimens are shown in Fig. 5a. Black, red, blue, and yellow curve represent neat DCPD, 1 wt%, 3 wt% and 5 wt% fiber loading DCPD composites, respectively. The strain was measured by the displacement between grips during the tensile testing corresponding to the original grip distance. The Young's modulus was determined by the slope of the elastic region with a strain rate of 0–2% of the original stress–strain curve. Toughness was obtained by integrating the areas under the original stress-strain curve. With the addition of CF, both tensile strength and breakage elongation were increased considerably, even though only limited amount of fibers was loaded. Both the tensile strength and Young's modulus of the composites increased with the increasing weight percent of d-CFs until 3 wt%. However, further notable enhancement by increasing CF loading was prohibited due to fiber aggregation and random orientation and increasing printing defects. Particularly, a higher CF fraction with random orientations introduced more significant disturbance in this extrusion and deposition process, such as nozzle gemming, resin-lacking in the deposited layers, and curing wave induced fiber orientation change, resulting in more defects to the printed sample. For a small-diameter nozzle, the printing layer is very thin and bead bonding between layers is more significant (fiber bundles lead to resin-lacking area, and thus bead bonding between printed layers). The fiber aggregation-induced defect proliferation in the printing process reduced the strength of sample. In the future work, further optimization of the process is needed for better control of the printing quality (fiber dispersion, synchronization of extrusion and frontal polymerization, layer size). The results of the tensile strength and Young's modulus results of DCPD and CF/DCPD composites are shown in Fig. 5b. DCPD

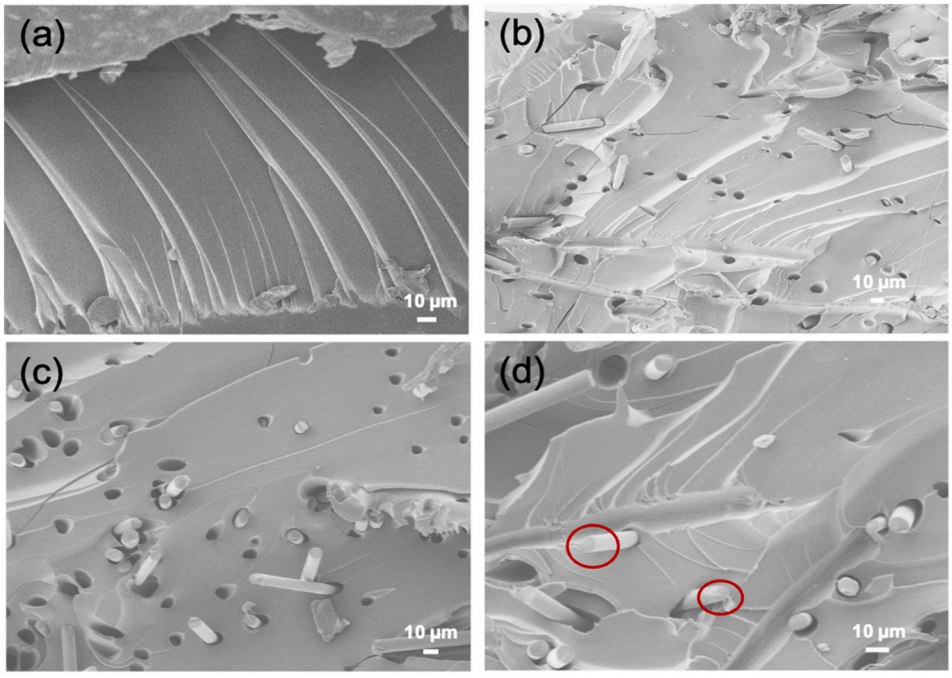

Fig. 9. SEM images of tensile test fracture surface of (a) neat DCPD; (b) sized CF/DCPD; (c) CF-COOH/DCPD; (d) CF-Nb/DCPD.

loaded with 3 wt% CFs exhibited the highest tensile strength. Compared to neat DCPD, the 3 wt%CF/ DCPD composites exhibited more than doubled tensile strength and an increase of ~72% in modulus compared to neat DCPD. DCPD with higher CF fractions showed a higher modulus because CF is highly rigid and strong, and it helps to improve the stiffness at an increasing fiber fraction.

According to results above, 3 wt% CF loading was selected to further study the effect of CF surface chemistry on the mechanical properties due to the dispersion challenge, as shown in Fig. 6. As-printed carboxyl-CF/DCPD also demonstrated tensile strength of 37.9 MPa, 1.3-fold enhancement with reference to neat resin. As-printed sized-CF/DCPD composites demonstrated tensile strength of 38.6MP, 1.4-fold enhancement in comparison with neat resin. The tensile strength of norbornene-CF composites was as high as 43.3MP, demonstrating 1.7-fold enhancement with reference to the neat resins. This was because the improved fiber/matrix interface with norbornene functionalization and the formation of covalent bonding between fiber and polymer matrix. The less-effective enhancement of Young's modulus for norbornene-CF/DCPD was caused by fiber shortening during to multi-step and long-time mechanical agitation and sonication dispersion.

Fibers subjected to different treatments were analyzed by an optical microscope, and their lengths were measured, as shown in Fig. S3, Table S1 and Fig. S4. Long fibers were found to be chopped during to the intensive mechanical agitation or sonication in the surface modification of norbornene while desizing and oxidation treatments did not affect the fiber length due to mild mechanical agitation. This is consistent with the reported literature that intensive mechanical agitation or sonication could synergistically work with chemical etching to significantly shorten the fibers [41]. In the future work, effective dispersion of fibers with only mild mechanical agitation or further simplifying process steps should be explored to avoid considerable fiber shortening while achieving the surface functionalization. Sample toughness and fracture strength were calculated and are shown in Fig. 6b. Obviously, norbornene-CFs significantly increased both the fracture strength and the toughness of the composites.

3.4. Interlayer bonding strength

The interlayer bonding was analyzed via a lap shear test. A two-layer specimen with 2mm^2 contact area was printed, as shown in the inset images a, b in Fig. 7. As-printed specimens were loaded to the tensile machine for lap shear test, as shown in inset image c in Fig. 7. Two ends of the specimen were griped and tightened in the load cell. Sandpapers were used to increase friction at the grips to hold the sample during the pulling process. The interlayer bonding strength results are shown in Fig. 7. The interlayer bonding strength of norbornene-CF/DCPD composites was significantly higher than that of neat DCPD resin. On average, the interlayer bonding strength of the norbornene-grafted fiber showed an improvement of ~133%, ~52% and ~ 255% with regard to carboxyl-grafted fiber/DCPD, sized-fiber/DCPD, and neat DCPD. FTIR analysis was carried out for characterizing those samples. The delaminated surface was analyzed under ATR-FTIR module. The results and descriptions are shown in Fig. S5 and Note S1. Interestingly, sized-CF filled composites exhibited a higher interlayer bonding strength than carboxyl-CF filled composite. This was attributed to the sizing agent coated on the fiber surface. The sizing usually contains a great number of active functional groups that can help improve wettability and affinity on fiber surface, thus, creating strong binding energy between polymer matrix and fibers [42]. The IR graph of CF with sizing agent is shown in Fig. 3c (green curve). On the other side, unitary surface modification of carboxyl group on the fiber surface along with oxygen-deprived alkene chain-dominated DCPD matrix weakened binding energy, compromising the interlayer bonding strength between carboxyl-CF and DCPD matrix.

The part height might significantly affect the thermally-activated interlayer bonding strength in the printed parts. During the printing, the heat loss via conduction was significant because as-deposited frontal-curing layers were in contact with room temperature substrate. Building upward, the heat loss problem may result in weakened frontal curing and diminished interlayer bonding at an increasing part height. We believe there are two strategies for overcoming this challenge toward printing true 3D parts(with dominant height), including (1) minimizing the conduction-based heat loss by minimizing contact between the substrate and printed structure or using highly-insulated

substrate, and (2) heating the substrate to counteract the heat loss by conduction. Frontal curing propagation in the air(e.g. spiral structure) has showed minimum heat loss through conduction, and thus the effect of part height on the thermally-activated bonding could be minimized if there is a minimum contact between the substrate and printed structure or an insulated substrate is used. In addition, the substrate could be heated during the printing process to compensate the heat loss by conduction, and thus the effect of part height on the thermally-activated bonding could be mitigated.

3.5. Cross-section structure characterization

The fracture surfaces of the lap shear test samples, including neat DCPD, sized CF/DCPD, CF-COOH/DCPD, CF-Nb/DCPD specimens, were characterized by SEM, and results are shown in the Fig. 8. It can be clearly observed the neat DCPD ones (Figure a, b) shows a smooth fracture surface compared to CFs-incorporated DCPD composites (Figure c-h), suggesting a weaker interaction between printed layers. On the other hand, rougher fracture surfaces of CF/DCPD composites represents an increased interlayer interactions and are subject to greater stress during the pull-out process. More significantly, in Fig. 8h, for Nb-CF/DCPD composites, many protruding fibers (marked by red circles) were observed on the fracture surface with strong adhesion of resin, indicating such Nb-CF short fibers ever bridged the printed interlayers for enhanced adhesive interactions between adjacent layers and also strong fiber-matrix interface. These observations are consistent with the interlayer bonding tests as shown in Fig. 7.

The protrusion fibers can be observed on the cross-section of tensile test specimens, as shown in Fig. 9. Similarly, the CF/DCPD composites showed a rougher cross-section surface with protrusion fiber and with numerous dimple structures compared to neat DCPD. Interestingly, compared to sized CF and COOH-CF in Fig. 9b and 9c, the fracture surface of protruded Nb-CF deformed to irregular shape, indicating that Nb-CFs endures higher load strength in the tensile stretching process, as shown in Fig. 9d. This is well-aligned with the tensile strength results shown in Fig. 5–6.

4. Conclusions

Lightweight short fiber/DCPD thermosetting composites were printed via frontal polymerization. The tensile strength of the printed norbornene-CF composites was around 43.3 MPa, which was 170% higher than printed neat DCPD resin and 15% higher than as-received sized-fiber/DCPD composites. The toughness of the printed composites was ~14 MPa, ~33.3% higher than printed sizing CF/DCPD composites. Moreover, the interlayer bonding strength of printed norbornene carbon fiber composites significantly was as high as 9.31 MPa, which was 255% increase compared to neat DCPD. The aforementioned experimental results demonstrated the effectiveness of adopting norbornene functionalized CF in enhancing the mechanical performance of printed DCPD composites. Further research needs to avoid fiber shortening during the surface modification process. Simplifying surface modification process, involving less agitative process and better fiber dispersion methods will be investigated in the near future to achieve effective surface functionalization while maintaining the original length, and thus significantly transforming the mechanical properties of printed thermosets.

Declaration of competing interest

There is no conflict of interest regarding this research.

Acknowledgements

We appreciate the funding support from National Science Foundation (CMMI-1934120, CMMI-1933679).

Appendix A. Supplementary data

Supplementary data to this article can be found online at https://doi.org/10.1016/j.jmapro.2021.10.014.

References

[1] Saba N, Jawaid M. A review on thermomechanical properties of polymers and fibers reinforced polymer composites. Journal of Industrial and Engineering Chemistry 2018;67:1–11.
[2] Supian ABM, Sapuan SM, Zuhri MYM, Zainudin ES, Ya HH. Hybrid reinforced thermoset polymer composite in energy absorption tube application: a review. Defence Technology 2018;14(4):291–305.
[3] Xu Z, Liang Y, Ma X, Chen S, Yu C, Wang Y, et al. Recyclable thermoset hyperbranched polymers containing reversible hexahydro-s-triazine. Nature Sustainability 2020;3(1):29–34.
[4] Pascault JP, Williams RJJ. Overview of thermosets: present and future. In: Thermosets, Elsevier; 2018. p. 3–34.
[5] Love LJ, Kunc V, Rios O, Duty CE, Elliott AM, Post BK, et al. The importance of carbon fiber to polymer additive manufacturing. Journal of Materials Research 2014;29(17):1893.
[6] Ngo TD, Kashani A, Imbalzano G, Nguyen KTQ, Hui D. Additive manufacturing (3D printing): a review of materials, methods, applications and challenges. Compos Part B Eng 2018;143:172–96.
[7] Ning F, Cong W, Hu Y, Wang H. Additive manufacturing of carbon fiber-reinforced plastic composites using fused deposition modeling: effects of process parameters on tensile properties. Journal of Composite Materials 2017;51(4):451–62.
[8] Ning F, Cong W, Qiu J, Wei J, Wang S. Additive manufacturing of carbon fiber reinforced thermoplastic composites using fused deposition modeling. Compos Part B Eng 2015;80:369–78.
[9] Parandoush P, Lin D. A review on additive manufacturing of polymer-fiber composites. Composite Structures 2017;182:36–53.
[10] Quan Z, Wu A, Keefe M, Qin X, Yu J, Suhr J, et al. Additive manufacturing of multi-directional preforms for composites: opportunities and challenges. Mater Today 2015;18(9):503–12.
[11] Tekinalp HL, Kunc V, Velez-Garcia GM, Duty CE, Love LJ, Naskar AK, et al. Highly oriented carbon fiber–polymer composites via additive manufacturing. Composites Science and Technology 2014;105:144–50.
[12] Kuang X, Zhao Z, Chen K, Fang D, Kang G, Qi HJ. High-speed 3D printing of high-performance thermosetting polymers via two-stage curing. Macromol Rapid Commun 2018;39(7):1700809.
[13] Park S, Smallwood AM, Ryu CY. Mechanical and thermal properties of 3D-printed thermosets by stereolithography. Journal of Photopolymer Science and Technology 2019;32(2):227–32.
[14] Campana C, Léger R, Sonnier R, Ferry L, Ienny P. Effect of post curing temperature on mechanical properties of a flax fiber reinforced epoxy composite. Compos A: Appl Sci Manuf 2018;107:171–9.
[15] Moreno M, Armentano I, Fortunati E, Mattioli S, Torre L, Lligadas G, et al. Cellulose nano-biocomposites from high oleic sunflower oil-derived thermosets. Eur Polym J 2016;79:109–20.
[16] Timmis AJ, Hodzic A, Koh L, Bonner M, Soutis C, Schäfer AW, et al. Environmental impact assessment of aviation emission reduction through the implementation of composite materials. Int J Life Cycle Assess 2015;20(2):233–43.
[17] Goli E, Parikh NA, Yourdkhani M, Hibbard NG, Moore JS, Sottos NR, et al. Frontal polymerization of unidirectional carbon-fiber-reinforced composites. Compos A: Appl Sci Manuf 2020;130:105689.
[18] Li F, Song Y, Yao M, Nie J, He Y. Design and properties of novel photothermal initiators for photoinduced thermal frontal polymerization. Polymer chemistry; 2020.
[19] Dean LM, Wu Q, Alshangiti O, Moore JS, Sottos NR. Rapid synthesis of elastomers and thermosets with tunable thermomechanical properties. ACS Macro Lett 2020; 9:819–24.
[20] Goli E, Gai T, Geubelle PH. Impact of boundary heat losses on frontal polymerization. J Phys Chem B 2020;124(29):6404–11.
[21] Kovacic S, Slugovc C. Ring-opening metathesis polymerisation derived poly (dicyclopentadiene) based materials. Materials Chemistry Frontiers 2020;4: 2235–55.
[22] Tran AD, Koch T, Knaack P, Liska R. Radical induced cationic frontal polymerization for preparation of epoxy composites. Compos A: Appl Sci Manuf 2020;132:105855.
[23] Mariani A, Fiori S, Chekanov Y, Pojman JA. Frontal ring-opening metathesis polymerization of dicyclopentadiene. Macromolecules 2001;34(19):6539–41.
[24] Robertson ID, Dean LM, Rudebusch GE, Sottos NR, White SR, Moore JS. Alkyl phosphite inhibitors for frontal ring-opening metathesis polymerization greatly increase pot life. ACS Macro Lett 2017;6(6):609–12.
[25] Lecompère M, Allonas X, Maréchal D, Criqui A. Versatility of pyrylium salt/vinyl ether initiating system for epoxide dual-cure polymerization: kick-starting effect of the coinitiator. Macromol Rapid Commun 2017;38(13):1600660.
[26] Fazende KF, Phachansitthi M, Mota-Morales JD, Pojman JA. Frontal polymerization of deep eutectic solvents composed of acrylic and methacrylic acids. J Polym Sci A Polym Chem 2017;55(24):4046–50.
[27] Fiori S, Mariani A, Ricco L, Russo S. First synthesis of a polyurethane by frontal polymerization. Macromolecules 2003;36(8):2674–9.

[28] Klikovits, N.; Liska, R.; D'Anna, A.; Sangermano, M., Successful UV-induced RICFP of epoxy-composites. Macromolecular Chemistry and Physics 2017, 218 (18).
[29] Ruiu A, Sanna D, Alzari V, Nuvoli D, Mariani A. Advances in the frontal ring opening metathesis polymerization of dicyclopentadiene. J Polym Sci A Polym Chem 2014;52(19):2776–80.
[30] Chen S, Tian Y, Chen L, Hu T. Epoxy resin/polyurethane hybrid networks synthesized by frontal polymerization. Chem Mater 2006;18(8):2159–63.
[31] Goli E, Robertson ID, Geubelle PH, Moore JS. Frontal polymerization of dicyclopentadiene: a numerical study. J Phys Chem B 2018;122(16):4583–91.
[32] Robertson ID, Yourdkhani M, Centellas PJ, Aw JE, Ivanoff DG, Goli E, et al. Rapid energy-efficient manufacturing of polymers and composites via frontal polymerization. Nature 2018;557(7704):223–7.
[33] Wang B, Arias KF, Zhang Z, Liu Y, Jiang Z, Sue H-J, et al. 3D printing of in-situ curing thermally insulated thermosets. Manufacturing Letters 2019;21:1–6.
[34] Papon EA, Haque A. Fracture toughness of additively manufactured carbon fiber reinforced composites. Addit Manuf 2019;26:41–52.
[35] Nawafleh N, Celik E. Additive manufacturing of short fiber reinforced thermoset composites with unprecedented mechanical performance. Addit Manuf 2020;33:101109.
[36] Yang F. Fire-retardant carbon-fiber-reinforced thermoset composites. In: Novel fire retardant polymers and composite materials, Elsevier; 2017. p. 271–93.
[37] Sheehan JE. Oxidation protection for carbon fiber composites. Carbon 1989;27(5):709–15.
[38] Vyas S, Goli E, Zhang X, Geubelle PH. Manufacturing of unidirectional glass-fiber-reinforced composites via frontal polymerization: a numerical study. Composites Science and Technology 2019;184:107832.
[39] Vyas S, Zhang X, Goli E, Geubelle PH. Frontal vs. bulk polymerization of fiber-reinforced polymer-matrix composites. Composites Science and Technology 2020;198:108303.
[40] Zhang Z, Liu R, Zepeda H, Zeng L, Qiu J, Wang S. 3D printing super strong hydrogel for artificial meniscus. ACS Applied Polymer Materials 2019;1(8):2023–32.
[41] Bussy C, Pinault M, Cambedouzou J, Landry MJ, Jegou P, Mayne-l'Hermite M, et al. Critical role of surface chemical modifications induced by length shortening on multi-walled carbon nanotubes-induced toxicity. Part Fibre Toxicol 2012;9(1):1–15.
[42] Zhang RL, Zhang JS, Zhao LH, Sun YL. Sizing agent on the carbon fibers surface and interface properties of its composites. Fibers and Polymers 2015;16(3):657–63.